Daily modulation due to channeling in direct dark matter crystalline detectors

Nassim Bozorgnia, Graciela B. Gelmini, and Paolo Gondolo

Phys. Rev. D **84**, 023516 — Published 13 July 2011

DOI: 10.1103/PhysRevD.84.023516

Daily modulation due to channeling in direct dark matter crystalline detectors

Nassim Bozorgnia,[1,*] Graciela B. Gelmini,[1,†] and Paolo Gondolo[2,‡]

[1]*Department of Physics and Astronomy, UCLA,*
475 Portola Plaza, Los Angeles, CA 90095, USA
[2]*Department of Physics, University of Utah,*
115 South 1400 East # 201, Salt Lake City, UT 84112, USA

Abstract

The channeling of the ion recoiling after a collision with a WIMP in direct dark matter crystalline detectors produces a larger scintillation or ionization signal than otherwise expected. Channeling is a directional effect which depends on the velocity distribution of WIMPs in the dark halo of our Galaxy and could lead to a daily modulation of the signal. Here we compute upper bounds to the expected amplitude of daily modulation due to channeling using channeling fractions that we obtained with analytic models in prior work. After developing the general formalism, we examine the possibility of finding a daily modulation due to channeling in the data already collected by the DAMA/NaI and DAMA/LIBRA experiments. We find that even the largest daily modulation amplitudes (of the order of 10% in some instances) would not be observable for WIMPs in the standard halo in the 13 years of data taken by the DAMA collaboration. For these to be observable the DAMA total rate should be 1/40 of what it is or the total DAMA exposure should be 40 times larger. The daily modulation due to channeling will be difficult to measure in future experiments. We find it could be observed for light WIMPs in solid Ne, assuming no background.

*Electronic address: nassim@physics.ucla.edu
†Electronic address: gelmini@physics.ucla.edu
‡Electronic address: paolo@physics.utah.edu

I. INTRODUCTION

The channeling effect in crystals refers to the orientation dependence of charged ion penetration in crystals. Channeling occurs when ions propagating in a crystal along symmetry axes and planes suffer a series of small-angle scatterings that maintain them in the open "channels" in between the rows or planes of lattice atoms and thus penetrate much further into the crystal than in other directions and loose all their energy into electrons. In dark matter crystalline detectors, a channeled ion recoiling after a collision with a WIMP (Weakly Interacting Massive Particle) would give all its energy to electrons, thus the quenching factor is $Q \simeq 1$ instead of the usual $Q < 1$ for a non-channeled ion. Thus channeling increases the ionization or scintillation signal expected from a WIMP. The potential importance of the channeling effect for direct dark matter detection was first pointed out for NaI (Tl) by Drobyshevski [1] and subsequently by the DAMA collaboration [2] in 2007. In 2008, Avignone, Creswick, and Nussinov [3] suggested that a daily modulation due to channeling could occur in NaI crystals, which would be a background free dark matter signature. Such a modulation of the rate due to channeling is expected to occur at some level because the "WIMP wind" arrives to Earth on average from a particular direction fixed to the Galaxy. Assuming that the dark matter halo is on average at rest with respect to the Galaxy, this is the direction towards which the Earth moves with respect to the Galaxy. Earth's daily rotation naturally changes the direction of the "WIMP wind" with respect to the crystal axes, thus changing the amount of recoiling ions that are channeled vs non-channeled. This amounts to a daily modulation of the dark matter signal detectable via scintillation or ionization.

Using analytic models of channeling which started to be developed in the 1960's, shortly after the effect was discovered, mostly by Lindhard [4] and collaborators, we recently computed channeling probabilities as function of the recoil energy E_R and initial direction $\hat{\mathbf{q}}$ of a recoiling ion in different materials [5, 6]. We used a recursion of the addition rule in probability theory (see Eq. 5.13 in Ref. [5]) to find the probability $\chi(E_R, \hat{\mathbf{q}})$ that a recoiling ion enters into any channel in terms of the channeling fractions for single channels $\chi_i(E_R, \hat{\mathbf{q}})$ that we computed (where the index i runs over all channels, both axial and planar). The channeling fractions for axial and planar channels are given in Eqs. 5.2 and 5.4 of Ref. [5], respectively.

In our previous papers [5, 6], we also obtained the "geometric" channeling fraction $P_{\rm geometric}(E_R)$ in the crystals we studied, by averaging the channeling probability $\chi(E_R, \hat{\mathbf{q}})$ over the initial recoil directions $\hat{\mathbf{q}}$ (assuming an isotropic distribution in $\hat{\mathbf{q}}$)

$$P_{\rm geometric}(E_R) = \frac{1}{4\pi} \int \chi(E_R, \hat{\mathbf{q}}) d\Omega_q. \tag{1}$$

This integral was computed using the Hierarchical Equal Area iso-Latitude Pixelization (HEALPix) [7] of the recoil direction sphere (see Appendix B of Ref. [5]). Here "geometric" refers to assuming that the distribution of recoil directions is isotropic. In reality, in a dark matter direct detection experiment, the distribution of recoil directions depends on the momentum distribution of the incoming WIMPs (see Section II).

Fig. 1.a and 1.b reproduced from Ref. [5], show respectively upper bounds to some channeling fractions for single channels $\chi_i(E_R, \hat{\mathbf{q}})$ for Na recoils (with $c = 1$) and geometric channeling fraction of Na and I recoiling ions in a NaI crystal at room temperature for 1 keV $< E_R <$ 20 keV. The parameter c mentioned in the figures is a number that we expect to be between 1 and 2, which regulates the importance of temperature corrections (for details see Ref. [5]). The channeling fractions are typically smaller for larger values of c thus setting $c = 0$, which is an unrealistic value, we get the largest upper bound to the channeling fractions that our calculations provide. In the figures we used $c = 0$ and $c = 1$. Notice also that the results in the figures do not take into account dechanneling effects which should also decrease the channeling fractions (we do not know how to properly take into account these effects with our analytic methods).

In this paper, we use the (upper bounds to the) channeling probability $\chi(E_R, \hat{\mathbf{q}})$ and the actual differential recoil spectrum to compute the event rate, taking into account channeled and non-channeled recoils (see Section III, in particular Eqs. 17 and 18 and compare them with Eq. 1). We then use this rate to compute upper bounds to the amplitude of the daily modulation due to channeling expected in NaI crystals. In Section IV, we examine the possibility that such a daily modulation might be observable in the data accumulated by the DAMA collaboration.

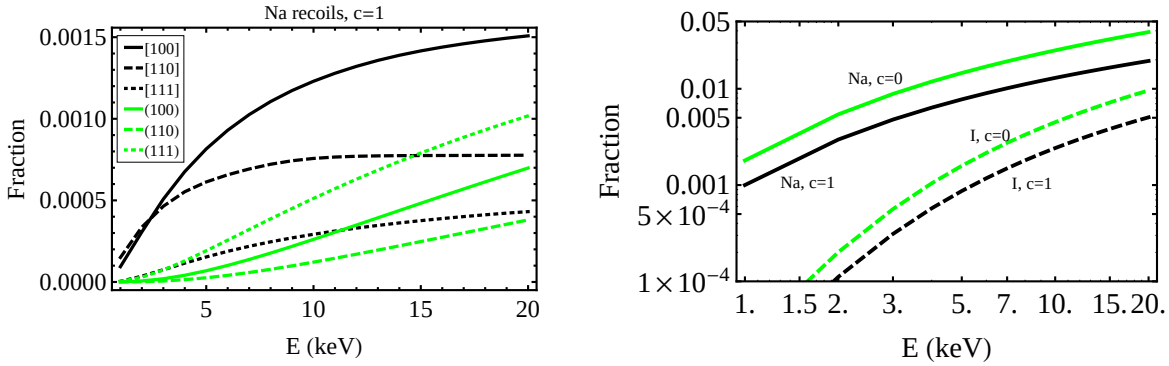

FIG. 1: (Color online) Upper bounds to the (a) channeling fractions for single channels $\chi_i(E, \hat{\mathbf{q}})$ of Na recoils for axial (black lines) and planar (green/gray lines) channels with $c = 1$, and (b) geometric channeling fraction $P_{\text{geometric}}(E)$ of Na (solid lines) and I recoils (dashed lines) as a function of the recoil energy E for $T = 293$ K in with $c = 0$ (green/gray) and $c = 1$ (black), always without including dechanneling.

II. ANGULAR DISTRIBUTION OF RECOIL DIRECTIONS DUE TO WIMPS

Consider the WIMP-nucleus elastic collision for a WIMP of mass m and a nucleus of mass M. The 3-dimensional "Radon transform" of the WIMP velocity distribution can be used to define the differential recoil spectrum as function of the recoil momentum $\vec{\mathbf{q}}$ [8]

$$\frac{dR}{dE_R\, d\Omega_q} = \frac{\rho\sigma_0 S(q)}{4\pi m\mu^2}\hat{f}_{\text{lab}}\left(\frac{q}{2\mu}, \hat{\mathbf{q}}\right), \tag{2}$$

where E_R is the recoil energy, $d\Omega_q = d\phi d\cos\theta$ denotes an infinitesimal solid angle around the recoil direction $\hat{\mathbf{q}} = \vec{\mathbf{q}}/q$, $q = |\vec{\mathbf{q}}|$ is the magnitude of the recoil momentum, $\mu = mM/(m+M)$ is the reduced WIMP-nucleus mass, $q/2\mu = v_q$ is the minimum velocity a WIMP must have to impart a recoil momentum q to the nucleus, or equivalently to deposit a recoil energy $E_R = q^2/2M$, ρ is the dark matter density in the solar neighborhood, σ_0 is the total scattering cross section of the WIMP with a (fictitious) point-like nucleus, and $S(q)$ is the nuclear form factor normalized to 1.

We concentrate here on WIMPs with spin-independent interactions, for which σ_0 is usually written in terms of the WIMP-proton cross section σ_p [9]

$$\sigma_0 = \frac{\mu^2}{\mu_p^2}A^2\sigma_p, \tag{3}$$

where $\mu_p = mm_p/(m+m_p)$ is the WIMP-proton reduced mass and A is the atomic number

of the nucleus. We use the Helm form factor [10]

$$S(q) = |F_{SI}(q)|^2 = \left(\frac{3j_1(qR_1)}{qR_1}\right)^2 e^{-q^2 s^2}, \tag{4}$$

where

$$j_1(x) = \frac{\sin x}{x^2} - \frac{\cos x}{x} \tag{5}$$

is the first kind spherical Bessel function, R_1 is an effective nuclear radius, and s is the nuclear skin thickness. Following Duda, Kemper, and Gondolo [11] we set

$$R_1 = \sqrt{c^2 + \frac{7}{3}\pi^2 a^2 - 5s^2}, \tag{6}$$

and take $s \simeq 0.9$ fm, $a \simeq 0.52$ fm, and $c \simeq (1.23A^{1/3} - 0.6)$ fm. These parameters have been chosen to match the numerical integration of the Two-Parameter Fermi model of nuclear density [11].

The Maxwellian WIMP velocity distribution with respect to the Galaxy, with dispersion σ_v and truncated at the escape speed $v_{\rm esc}$ is given by [8]

$$f_{\rm WIMP}(\mathbf{v}) = \frac{1}{N_{\rm esc}(2\pi\sigma_v^2)^{3/2}} \exp\left[-\frac{(\mathbf{v}+\mathbf{V}_{\rm lab})^2}{2\sigma_v^2}\right], \tag{7}$$

for $|\mathbf{v} + \mathbf{V}_{\rm lab}| < v_{\rm esc}$, and zero otherwise, where

$$N_{esc} = \mathrm{erf}\left(\frac{v_{\rm esc}}{\sqrt{2}\sigma_v}\right) - \sqrt{\frac{2}{\pi}}\frac{v_{\rm esc}}{\sigma_v} \exp\left[-\frac{v_{\rm esc}^2}{2\sigma_v^2}\right]. \tag{8}$$

Here we are assuming the detector has a velocity $\mathbf{V}_{\rm lab}$ with respect to the Galaxy (thus $-\mathbf{V}_{\rm lab}$ is the average velocity of the WIMPs with respect to the detector). $\mathbf{V}_{\rm lab}$ is defined in terms of the galactic rotation velocity $\mathbf{V}_{\rm GalRot}$ at the position of the Sun (or Local Standard of Rest (LSR) velocity), Sun's peculiar velocity $\mathbf{V}_{\rm Solar}$ in the LSR, Earth's translational velocity $\mathbf{V}_{\rm EarthRev}$ with respect to the Sun, and the velocity of Earth's rotation around itself $\mathbf{V}_{\rm EarthRot}$ (see Appendix B),

$$\mathbf{V}_{\rm lab} = \mathbf{V}_{\rm GalRot} + \mathbf{V}_{\rm Solar} + \mathbf{V}_{\rm EarthRev} + \mathbf{V}_{\rm EarthRot}. \tag{9}$$

In this paper we take $V_{\rm GalRot}$ either 220 km/s or 280 km/s, as reasonable low and high values (as done in Ref [12]), which correspond to $V_{\rm lab}$ either 228.4 km/s or 288.3 km/s, respectively (see Appendix B for details). Ref. [13] gives 100 km/s as the smallest estimate for the 1D velocity dispersion, which corresponds to a 3D dispersion $\sqrt{3}$ times larger, i.e. $\sigma_v = 173$ km/s. Thus here we take σ_v either 173 km/s or 300 km/s [8].

In order to visualize the arrival directions of WIMPs, we will plot $f_{\rm WIMP}(\hat{\mathbf{v}}, v_q)$, the number of WIMPs per solid angle in the direction $\hat{\mathbf{v}}$ in several figures. If we limit ourselves to the WIMPs with speed higher than v_q, then

$$f_{\rm WIMP}(\hat{\mathbf{v}}, v_q) = \int_{v_q}^{v_{\rm max}(\hat{\mathbf{v}})} f_{\rm WIMP}(\mathbf{v}) v^2 dv. \tag{10}$$

The upper limit of the integral in Eq. 10 is such that $|\mathbf{v} + \mathbf{V}_{\rm lab}| = v_{\rm esc}$ and depends on the direction $\hat{\mathbf{v}}$, since $(\mathbf{v} + \mathbf{V}_{\rm lab})^2 = v^2 + 2v\ \hat{\mathbf{v}}.\mathbf{V}_{\rm lab} + V_{\rm lab}^2$,

$$v_{\rm max}(\hat{\mathbf{v}}) = -\hat{\mathbf{v}}.\mathbf{V}_{\rm lab} + \sqrt{(\hat{\mathbf{v}}.\mathbf{V}_{\rm lab})^2 - \mathbf{V}_{\rm lab}^2 + v_{\rm esc}^2}\ , \tag{11}$$

and

$$f_{\rm WIMP}(\hat{\mathbf{v}}, v_q) = \frac{\exp\left(-\frac{V_{\rm lab}^2}{2\sigma_v^2}\right)}{N_{\rm esc}(2\pi\sigma_v^2)^{3/2}} \int_{v_q}^{v_{\rm max}(\hat{\mathbf{v}})} \exp\left(\frac{-v^2}{2\sigma_v^2}\right) \exp\left(\frac{-2v\ \hat{\mathbf{v}}.\mathbf{V}_{\rm lab}}{2\sigma_v^2}\right) v^2 dv. \tag{12}$$

This integral can be solved analytically and the result is in terms of error functions,

$$\begin{aligned} f_{\rm WIMP}(\hat{\mathbf{v}}, v_q) = \frac{\exp\left(-\frac{V_{\rm lab}^2}{2\sigma_v^2}\right)}{N_{\rm esc}(2\pi\sigma_v^2)^{3/2}} \left(\frac{\sigma_v}{2}\right) \Bigg\{ & \sqrt{2\pi}\left[(\hat{\mathbf{v}}.\mathbf{V}_{\rm lab})^2 + \sigma_v^2\right] \exp\left(\frac{(\hat{\mathbf{v}}.\mathbf{V}_{\rm lab})^2}{2\sigma_v^2}\right) \\ & \left[\mathrm{erf}\left(\frac{\hat{\mathbf{v}}.\mathbf{V}_{\rm lab} + v_{\rm max}(\hat{\mathbf{v}})}{\sqrt{2}\sigma_v}\right) - \mathrm{erf}\left(\frac{\hat{\mathbf{v}}.\mathbf{V}_{\rm lab} + v_q}{\sqrt{2}\sigma_v}\right)\right] \\ & + (2\sigma_v)\Bigg[(\hat{\mathbf{v}}.\mathbf{V}_{\rm lab} - v_{\rm max}(\hat{\mathbf{v}})) \exp\left(-\frac{v_{\rm max}(\hat{\mathbf{v}})(2\hat{\mathbf{v}}.\mathbf{V}_{\rm lab} + v_{\rm max}(\hat{\mathbf{v}}))}{2\sigma_v^2}\right) \\ & + (-\hat{\mathbf{v}}.\mathbf{V}_{\rm lab} + v_q) \exp\left(-\frac{v_q(2\hat{\mathbf{v}}.\mathbf{V}_{\rm lab} + v_q)}{2\sigma_v^2}\right)\Bigg]\Bigg\}. \end{aligned} \tag{13}$$

The maximum of $f_{\rm WIMP}(\hat{\mathbf{v}}, v_q)$ happens when $\hat{\mathbf{v}}.\mathbf{V}_{\rm lab} = -V_{\rm lab}$, i.e. in the direction of the "WIMP wind" average velocity $-\mathbf{V}_{\rm lab}$. Dividing $f_{\rm WIMP}(\hat{\mathbf{v}}, v_q)$ by this maximum we obtain a re-scaled distribution, a dimensionless number between 0 and 1, which we plot in Fig. 2 (see the color scale/grayscale in the figure) on the sphere of velocity directions $\hat{\mathbf{v}}$ using the HEALPix pixelization [7] (see also Appendix B of Ref. [5]) for all WIMPs, which amounts to taking $v_q = 0$. We took $V_{\rm lab} = 288.3$ km/s, and $\sigma_v = 300$ km/s or $\sigma_v = 173$ km/s for Fig. 2.a or b respectively.

For a truncated Maxwellian WIMP velocity distribution with respect to the Galaxy, truncated at the escape speed $v_{\rm esc}$, the Radon-transform is [8]

$$\hat{f}_{\rm lab}\left(\frac{q}{2\mu}, \hat{\mathbf{q}}\right) = \frac{1}{N_{\rm esc}(2\pi\sigma_v^2)^{1/2}} \left\{ \exp\left[-\frac{\left[(q/2\mu) + \hat{\mathbf{q}}.\mathbf{V}_{\rm lab}\right]^2}{2\sigma_v^2}\right] - \exp\left[\frac{-v_{\rm esc}^2}{2\sigma_v^2}\right]\right\}, \tag{14}$$

if $(q/2\mu) + \hat{\mathbf{q}}.\mathbf{V}_{\rm lab} < v_{\rm esc}$, and zero otherwise.

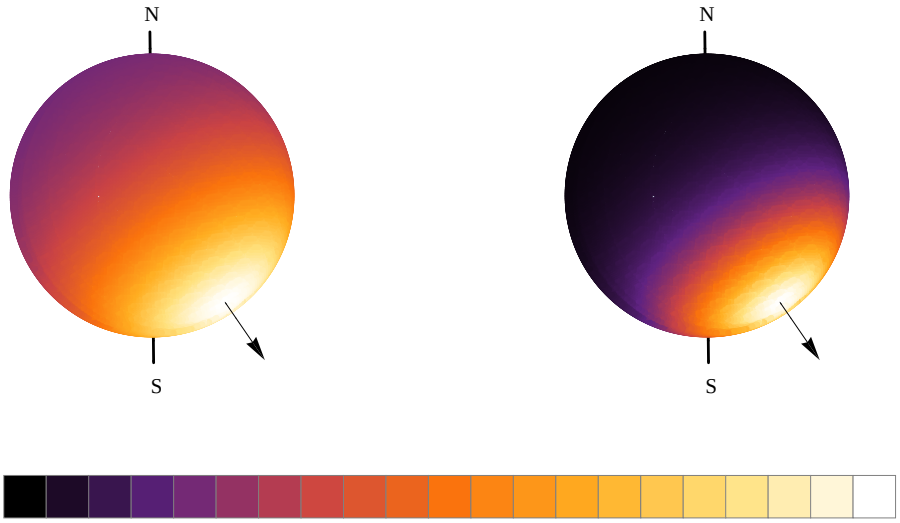

FIG. 2: (Color online) WIMPs number density per solid angle $f_{\rm WIMP}(\hat{\mathbf{v}}, v_q)$ (in Eq. 13) for all WIMPs (namely $v_q = 0$) re-scaled to be a number between 0 (black) and 1 (white) plotted on the sphere of velocity directions $\hat{\mathbf{v}}$ using the HEALPix pixelization for $V_{\rm lab} = 288.3$ km/s and (a) $\sigma_v = 300$ km/s and (b) $\sigma_v = 173$ km/s. The arrow shows the direction of the average velocity of the WIMP wind, $-\mathbf{V}_{\rm lab}$. The North and South celestial poles are also indicated. The color scale/grayscale shown in the horizontal bar between black and white corresponds to values between 0 and 1 in increments of 0.05.

The presence of $\hat{\mathbf{q}}.\mathbf{V}_{\rm lab}$ means that in order to compute the differential rate we need to orient the nuclear recoil direction $\hat{\mathbf{q}}$ with respect to $\mathbf{V}_{\rm lab}$.

The maximum of $\hat{f}_{\rm lab}(\frac{q}{2\mu}, \hat{\mathbf{q}})$ in Eq. 14 happens when $\hat{\mathbf{q}}.\mathbf{V}_{\rm lab} = -q/2\mu$, if $v_q = q/2\mu < V_{\rm lab}$ (or in the direction of $-\mathbf{V}_{\rm lab}$ otherwise). Thus, we can re-scale $\hat{f}_{\rm lab}$ to obtain a dimensionless number between 0 and 1,

$$\hat{f}_{\rm lab}^{\rm re-scaled} = \left\{ \exp\left[-\frac{\left[(q/2\mu) + \hat{\mathbf{q}}.\mathbf{V}_{\rm lab}\right]^2}{2\sigma_v^2} \right] - \exp\left[\frac{-v_{\rm esc}^2}{2\sigma_v^2} \right] \right\} \Big/ \left(1 - \exp\left[\frac{-v_{\rm esc}^2}{2\sigma_v^2} \right] \right). \qquad (15)$$

In Figs. 3 and 4 we present side by side the WIMPs velocity distribution, for WIMPs which can generate a signal of a certain energy E, namely with speed above v_q (left panels) and the Radon transform (right panels) of the recoils of energy E that WIMP collisions produce.

In Fig. 3.a and b we respectively plot $f_{\rm WIMP}(\hat{\mathbf{v}}, v_q)$ on the sphere of WIMP velocity

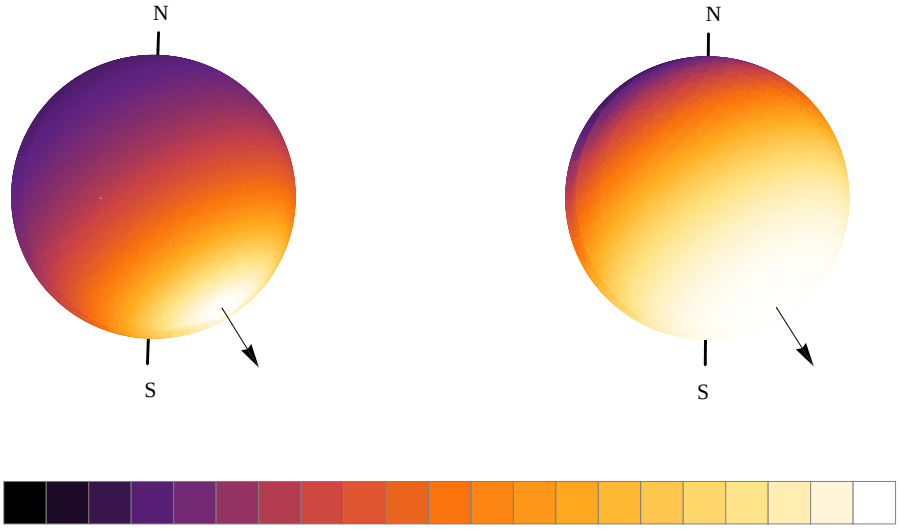

FIG. 3: (Color online) (a) $f_{\rm WIMP}(\hat{\mathbf{v}}, v_q)$ (in Eq. 13) re-scaled to be between 0 and 1 plotted on the sphere of velocity directions $\hat{\mathbf{v}}$ and (b) $\hat{f}_{\rm lab}$ (re-scaled as in Eq. 15) plotted on the sphere of recoil directions using the HEALPix pixelization for I recoils with $E_R = 10$ keV, $m = 30$ GeV (thus $v_q = 304.6$ km/s), $V_{\rm lab} = 288.3$ km/s and $\sigma_v = 300$ km/s. The arrow shows the direction of the average velocity of the WIMP wind, $-\mathbf{V}_{\rm lab}$. The North and South celestial poles are also indicated. The color scale/grayscale shown in the horizontal bar corresponds to values between 0 (black) and 1 (white) in intervals of 0.05.

directions $\hat{\mathbf{v}}$ and $\hat{f}_{\rm lab}$ on the sphere of recoil directions (both re-scaled to be a number between 0 and 1) using the HEALPix pixelization [7] for I recoils assuming $V_{\rm lab} = 288.3$ km/s, $E_R = 10$ keV, $\sigma_v = 300$ km/s and $m = 30$ GeV. Fig. 4.a and b show the same two distributions but for Na recoils and assuming $\sigma_v = 173$ km/s and $m = 60$ GeV (other parameters are the same). The color scale/grayscale plotted on the spheres indicate different values of the rescaled distributions: between 0 (black) and 1 (white) in intervals of 0.05. In Fig. 3 the minimum WIMP speed required is $v_q = 304.6$ km/s (I recoils), and since $v_q > V_{\rm lab}$, the maximum value of $\hat{f}_{\rm lab}^{\rm re-scaled}$, i.e. the maximum recoil rate, is in the direction of the "WIMP wind" average velocity, $-V_{\rm lab}$, which is shown with an arrow. In Fig. 4 instead, $v_q = 196.7$ km/s (Na recoils) and the maximum value of $\hat{f}_{\rm lab}^{\rm re-scaled}$ occurs when $-\hat{\mathbf{q}}.\mathbf{V}_{\rm lab} = v_q$, i.e. when $\hat{\mathbf{q}}$ is at an angle of 47° of $-V_{\rm lab}$.

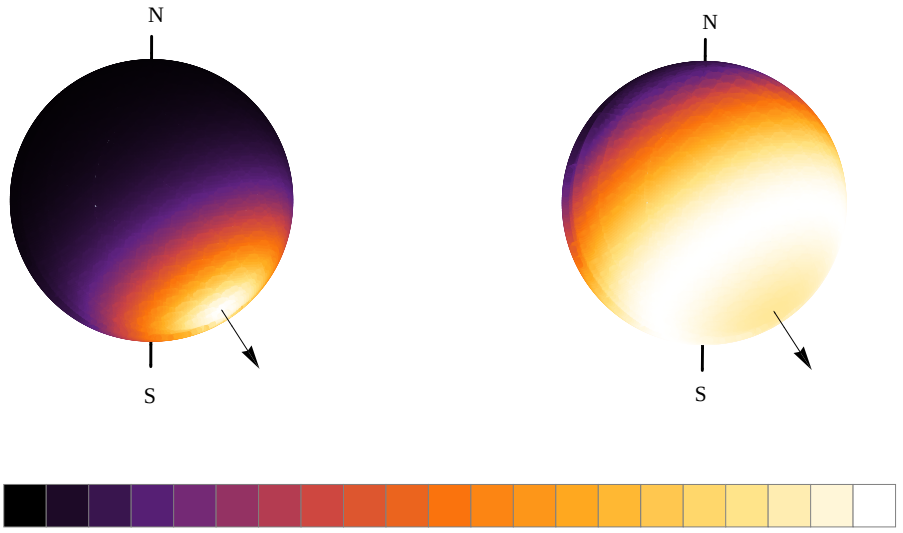

FIG. 4: (Color online) Same as Fig. 3 but for Na recoils and assuming $m = 60$ GeV (so $v_q = 196.7$ km/s) and $\sigma_v = 173$ km/s (and all other parameters the same).

III. DIFFERENTIAL ENERGY SPECTRUM

Let $p(E, E_R, \hat{\mathbf{q}})dE$ be the probability that an energy E is measured when a nucleus recoils in the direction $\hat{\mathbf{q}}$ with initial energy E_R, normalized so that

$$\int p(E, E_R, \hat{\mathbf{q}})dE = 1. \tag{16}$$

With our analytic approach we cannot estimate the importance of dechanneling mechanisms, such as the presence of lattice imperfections, impurities or dopants. Thus we disregard dechanneling, and assume that a recoiling nucleus can only either be channeled, in which case the measured energy is the whole initial recoil energy $E = E_R$ (first term in the following equation) or not channeled, in which case the measured energy is $E = QE_R$ (second term),

$$p(E, E_R, \hat{\mathbf{q}}) = \chi(E_R, \hat{\mathbf{q}})\delta(E - E_R) + [1 - \chi(E_R, \hat{\mathbf{q}})]\delta(E - QE_R). \tag{17}$$

The first term accounts for the channeled (unquenched) events and the second term for the unchanneled (quenched) events, and Q is the quenching factor.

Using Eq. 17 the differential energy spectrum,

$$\frac{dR}{dE} = \int \frac{dR}{dE_R d\Omega_q} p(E, E_R, \hat{\mathbf{q}})d\Omega_q dE_R, \tag{18}$$

can be written as

$$\frac{dR}{dE} = \int \left[\chi(E,\hat{\mathbf{q}}) \left.\frac{dR}{dE_R d\Omega_q}\right|_{E_R=E} + [1-\chi(E/Q,\hat{\mathbf{q}})] \frac{1}{Q} \left.\frac{dR}{dE_R d\Omega_q}\right|_{E_R=E/Q} \right] d\Omega_q$$
$$= \left.\frac{dR}{dE}\right|_{\rm U} + \int \left[\chi(E,\hat{\mathbf{q}}) \left.\frac{dR}{dE_R d\Omega_q}\right|_{E_R=E} - \chi(E/Q,\hat{\mathbf{q}}) \frac{1}{Q} \left.\frac{dR}{dE_R d\Omega_q}\right|_{E_R=E/Q} \right] d\Omega_q, \quad (19)$$

where the differential recoil spectrum with subindex "U", which stands for "Usual" (i.e. when channeling is not taken into account) is

$$\left.\frac{dR}{dE}\right|_{\rm U} = \int \frac{1}{Q} \left.\frac{dR}{dE_R d\Omega_q}\right|_{E_R=E/Q} d\Omega_q = \frac{1}{Q} \left.\frac{dR}{dE_R}\right|_{E_R=E/Q}. \quad (20)$$

Defining $\tilde{q} \equiv \sqrt{2EM}$ and using Eq. 2, the measured differential rate becomes,

$$\frac{dR}{dE} = \left.\frac{dR}{dE}\right|_{\rm U} + \frac{\rho\sigma_0}{4\pi m\mu^2} \left[S(\tilde{q}) \int \chi(E,\hat{\mathbf{q}}) \hat{f}_{\rm lab}\left(\frac{\tilde{q}}{2\mu},\hat{\mathbf{q}}\right) d\Omega_q \right.$$
$$\left. - \frac{S(\tilde{q}/\sqrt{Q})}{Q} \int \chi(E/Q,\hat{\mathbf{q}}) \hat{f}_{\rm lab}\left(\frac{\tilde{q}}{2\mu\sqrt{Q}},\hat{\mathbf{q}}\right) d\Omega_q \right]. \quad (21)$$

Inserting σ_0 from Eq. 3 in the above equation with the usual value for the mean local halo density $\rho = 0.3$ GeV/cm^3, we can write the spin-independent detection rate of WIMPs in general for a crystal that may contain more than one element

$$\frac{dR}{dE} = \left.\frac{dR}{dE}\right|_{\rm U} + 1.306\times10^{-3} \frac{\text{events}}{\text{kg-day-keV}} \times \frac{\sigma_{44}}{4\pi m\mu_p^2} \sum_n C_n A_n^2 \left[S(\tilde{q}) \int \chi_n(E,\hat{\mathbf{q}}) \hat{f}_{\rm lab}\left(\frac{\tilde{q}}{2\mu_n},\hat{\mathbf{q}}\right) d\Omega_q \right.$$
$$\left. - \frac{S(\tilde{q}/\sqrt{Q_n})}{Q_n} \int \chi_n(E/Q_n,\hat{\mathbf{q}}) \hat{f}_{\rm lab}\left(\frac{\tilde{q}}{2\mu_n\sqrt{Q_n}},\hat{\mathbf{q}}\right) d\Omega_q \right], \quad (22)$$

where σ_{44} is the WIMP-proton cross section in units of 10^{-44} cm^2, μ_p and m are in GeV and $\int \hat{f}_{\rm lab} d\Omega_q$ is in (km/s)$^{-1}$. The sum is over the nuclear species n in a crystal, and C_n, χ_n, Q_n and μ_n are the mass fraction, the channeling probability, the quenching factor and the reduced WIMP-nucleus mass for the element n, respectively. For example, for NaI crystals, as used in the DAMA experiment, we have $C_{\rm Na} = M_{\rm Na}/(M_{\rm Na}+M_{\rm I})$ and $C_{\rm I} = M_{\rm I}/(M_{\rm Na}+M_{\rm I})$, where $M_{\rm Na}$ and $M_{\rm I}$ are the atomic masses of Sodium and Iodine respectively.

The integrals in Eq. 22 cannot be computed analytically. We integrate numerically by performing a Riemann sum once the sphere of directions has been divided using HEALPix [7] (see also Appendix B of Ref. [5]). HEALPix provides a convenient way of dividing the surface of a sphere into equal area sectors, and in our papers [5, 6] we use it for the first time to compute integrals over directions.

With the same notation, the usual rate is

$$\left.\frac{dR}{dE}\right|_{\rm U} = 1.306{\times}10^{-3}\frac{\rm events}{\rm kg\text{-}day\text{-}keV}{\times}\frac{\sigma_{44}}{4\pi m\mu_p^2}\sum_n C_n\,A_n^2\,\left[\frac{S(\tilde{q}/\sqrt{Q_n})}{Q_n}\int \hat{f}_{\rm lab}\left(\frac{\tilde{q}}{2\mu_n\sqrt{Q_n}},\hat{\mathbf{q}}\right)d\Omega_q\right]. \tag{23}$$

IV. DAILY MODULATION IN NAI CRYSTALS

We present here the daily modulation amplitude due to channeling expected in NaI crystals for several WIMP masses and Na or I recoil energies. We assume that WIMPs have a truncated Maxwellian velocity distribution as in Eq. 7 with $v_{\rm esc} = 650$ km/s. We use the upper bounds to channeling fractions for single channels $\chi_i(E_R, \hat{\mathbf{q}})$ given in Ref. [5]. We take $T = 293$ K, the temperature of the DAMA experiment.

The spin-independent detection rate of WIMPs given in Eq. 22 has a time dependence through the Radon transform $\hat{f}_{\rm lab}$. Notice that $\hat{f}_{\rm lab}$ (see Eq. 14) changes during a day through the $(\hat{\mathbf{q}}.\mathbf{V}_{\rm lab})$ factor appearing in the exponent and the dependence of $\mathbf{V}_{\rm lab}$ on $\mathbf{V}_{\rm EarthRot}$ (see Eq. 9). The expression showing the time dependence of $\hat{\mathbf{q}}.\mathbf{V}_{\rm lab}$ is given in Eq. B13 (in Appendix B). During a day, $\mathbf{V}_{\rm EarthRev}$ which is responsible for the annual modulation changes too. Thus the rate does not return to exactly the same value after one day. For the cases we present in this paper, this difference is less than 10% of the total modulation amplitude in a day, and we did not correct for this effect.

A. Relative Modulation Amplitudes

Here we show the signal rate as function of time during a particular arbitrary Solar day (September 25, 2010). We define the relative signal modulation amplitude A_s (taking into account the signal only) in terms of the maximum and minimum daily signal rate R_s as

$$A_s = \frac{R_{s-\rm max} - R_{s-\rm min}}{R_{s-\rm max} + R_{s-\rm min}}. \tag{24}$$

The total relative modulation amplitude A_T is defined in terms of the maximum $R_{T-\rm max}$ and minimum $R_{T-\rm min}$ total daily rates as

$$A_T = \frac{R_{T-\rm max} - R_{T-\rm min}}{R_{T-\rm max} + R_{T-\rm min}}. \tag{25}$$

The total rate consists of signal plus background, $R_T = R_s + R_b$. Assuming that there is no daily modulation in the background, $R_{T-\max} - R_{T-\min} = R_{s-\max} - R_{s-\min}$, and A_T is related to A_s as

$$A_T = A_s(R_s/R_T), \tag{26}$$

where the average total rate due to signal and background is $R_T = (R_{T-\max} + R_{T-\min})/2$ and the average rate due to the signal alone is $R_s = (R_{s-\max} + R_{s-\min})/2$.

Exploring the parameter space of WIMP mass and WIMP-proton cross section for different recoil energies we find that the relative modulation amplitudes A_s can be large, even more than 10% for some combination of parameters. We explored the range of WIMP masses from a few GeV to hundreds of GeV for recoil energies between 2 keV and a few MeV. We show some examples in Fig. 5, where we plot the signal rate (in events/kg/day/keVee) as function of the Universal Time (UT) during 24 hours. We find that the largest A_s happen when the signal is only due to channeling. This happens when there are no WIMPs in the galactic halo with large enough kinetic energy to provide the observed energy if the recoil is not channeled. The observed energies for which the rate is only due to channeling depend on the quenching factors Q, which are not well known. The smaller values of Q make channeling more important so we take $Q_{\rm Na} = 0.2$ [16] for Na and the usual $Q_{\rm I} = 0.09$ for I.

B. Statistical Significance

The detectability of a particular amplitude of daily modulation depends on the exposure and background of a particular experiment. The former DAMA/NaI and the DAMA/LIBRA experiments (which we refer collectively as the DAMA experiment) have a very large cumulative exposure, 1.17 ton $\times$ year. However even with this large exposure, we find that the daily modulations we predict are not observable. To observe the daily modulation, the total number of events N_T (N_s signal plus N_b background events) over the duration of the experiment should be divided into two bins, the "high-rate" bin with $N_{T-\max}$ events and the "low-rate" bin with $N_{T-\min}$ events, so that $N_T = N_{T-\max} + N_{T-\min}$. For the daily modulation to be observable at, say, the 3σ level one should have

$$N_{T-\max} - N_{T-\min} = A_T N_T > 3\sigma \simeq 3\sqrt{N_T/2}, \tag{27}$$

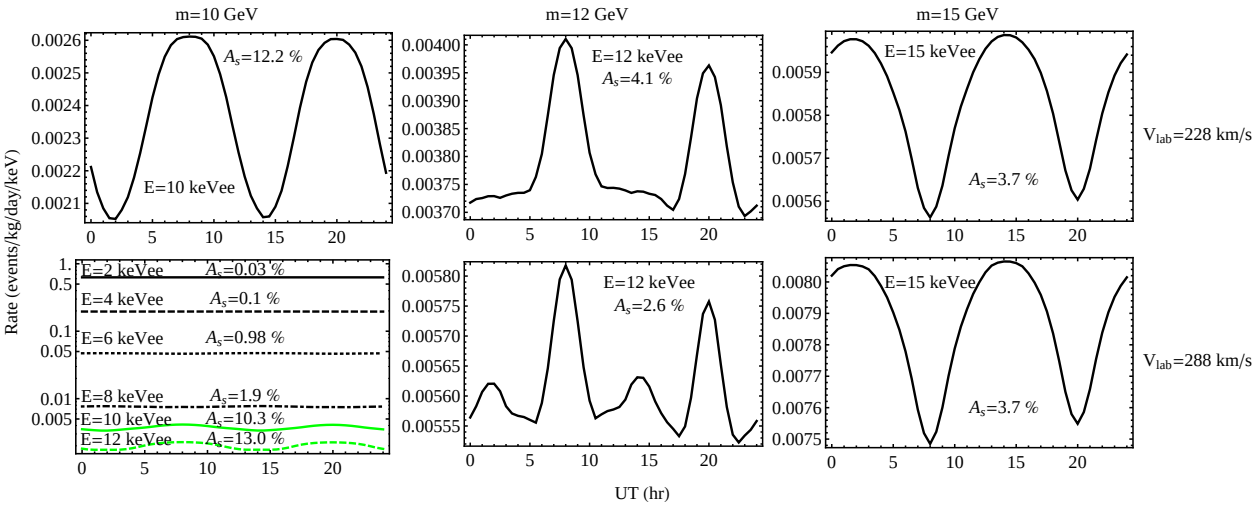

FIG. 5: Signal rate (in events/kg-day-keVee) as function of the Universal Time (UT) during 24 hours for $m = 10$ GeV, 12 GeV and 15 GeV for different energies. The parameters used are $\sigma_v = 300$ km/s, $Q_{\rm Na} = 0.2$, $Q_{\rm I} = 0.09$, $\sigma_p = 2 \times 10^{-40}{\rm cm}^2$, $c = 1$ for temperature effects, a crystal temperature of $T = 293$ K and $V_{\rm lab} = 228.4$ km/s (top row) or 288.3 km/s (bottom row).

where $\sigma^2 \simeq N_T/2$ because, with a small modulation, on average $N_{T-\rm max} \simeq N_{T-\rm min} \simeq N_T/2$. In principle there are other errors associated with identifying the "high-rate" and "low-rate" bins which we do not include here. Thus we are underestimating the errors.

If the detector exposure is MT in kg-day and we take bins of width ΔE in keVee, then $N_{T-\rm max} = R_{T-\rm max} MT\Delta E/2$, $N_{T-\rm min} = R_{T-\rm min} MT\Delta E/2$, $N_T = R_T MT\ \Delta E$ and $N_s = R_s MT\Delta E$, where the rates are in events/kg-day-keVee. Thus $(N_s/N_T) = (R_s/R_T)$ and using Eq. 26, $A_T = A_s(N_s/N_T)$. Thus the condition in Eq. 27 becomes $A_s N_s > 3\sqrt{N_T/2}$ which implies

$$N_s^2/N_T > 9/(2A_s^2), \tag{28}$$

or

$$R_s^2/R_T > 9/(2A_s^2 MT\ \Delta E). \tag{29}$$

The total rate of the DAMA experiment at low energies 4 keVee $< E <$ 10 keVee is $R_T \simeq 1$ events/kg/day/keVee [14]. This rate is much larger than the signal rates we predict and is, therefore, dominated by background. With this value of R_T, Eq. 29 becomes

$$R_s^2 A_s^2 > \frac{9}{2MT\ \Delta E\ {\rm kg\ day\ keVee}}. \tag{30}$$

We choose here a bin $\Delta E \simeq 1$ keVee, narrow enough to assume the signal rate to be constant in it and compatible with the energy resolution of DAMA. The energy resolution of DAMA is $\sigma_E(E) = (0.448 \text{ keVee})\sqrt{E/\text{keVee}} + (0.0091)E \simeq 1$ keVee at low energies [15]. We consider the significance of the highest signal-to-noise energy bin that we found through inspection. With the cumulative exposure of DAMA, the condition in Eq. 30 for relative daily modulation amplitudes A_s observable at 3σ is

$$R_s \; A_s > 3.2 \times 10^{-3} \text{ events/kg/day/keVee}, \tag{31}$$

or

$$R_{s-\max} - R_{s-\min} > 6.4 \times 10^{-3} \text{ events/kg/day/keVee}. \tag{32}$$

For observability at the $n\sigma$ level we should multiply the right-hand side of Eq. 32 by $(n/3)$. Even the largest relative daily modulations we find, shown in Fig. 5, are not observable in the DAMA data according to Eq. 32.

The examples which we show here are for small WIMP masses and recoil energies. For large masses the value of σ_p must be chosen in the region of the cross section and mass plane where XENON10/100 and CDMS impose σ_p to be smaller by four orders of magnitude than for light WIMPs. This amounts to corresponding smaller signal rates and $(R_{s-\max} - R_{s-\min})$ differences. For small WIMP masses and large energies, v_q is large and there are no WIMPs with the speed required for Na or I recoils. Thus, only small WIMP masses and recoil energies result in high modulation amplitudes.

Fig. 5 shows the signal rate during 24 hours for three different WIMP masses $m = 10$ GeV, 12 GeV and 15 GeV and different energies E between 2 and 15 keVee. The other relevant parameters are $\sigma_v = 300$ km/s, $\sigma_p = 2 \times 10^{-40}\text{cm}^2$ (close to the DAMA and CoGeNT regions [16–18]), $c = 1$, $T = 293$ K and two values of V_{lab}, 228.4 km/s (top row) and 288.3 km/s (bottom row). Recent bounds, e.g. those from XENON100 [19], impose smaller values of σ_p. In any event, changes in σ_p are easy to take into account because A_s is independent of σ_p and the rate is just proportional to it, $R_s \sim \sigma_p$.

We found the relative amplitude A_s to be as large as 12% in the examples shown in Fig. 5, but even those large values are not observable according to Eq. 32 (even at the 1σ level). With the choice of $V_{\text{lab}} = 228.4$ km/s (top row of Fig. 5) we get a signal rate difference $R_{s-\max} - R_{s-\min}$ of 0.56×10^{-3} events/kg/day/keVee for $m = 10$ GeV and $E = 10$ keVee (in this case $v_q = 454.8$ km/s and 790.5 km/s for channeled Na and I recoils, respectively),

3.17×10^{-4} events/kg/day/keVee for $m = 12$ GeV and $E = 12$ keVee (which corresponds to $v_q = 441.6$ km/s and 732.9 km/s for Na and I channeled recoils, respectively), and 4.25×10^{-4} events/kg/day/keVee for $m = 15$ GeV and $E = 15$ keVee (for which $v_q = 430.6$ km/s and 670.6 km/s for Na and I channeled recoils, respectively). With the choice of $V_{\rm lab} = 288.3$ km/s (bottom row of Fig. 5), $R_{s-\max} - R_{s-\min}$ is 0.77×10^{-3} events/kg/day/keVee for $m = 10$ GeV and $E = 10$ keVee (one of the energies shown), 2.95×10^{-4} events/kg/day/keVee for $m = 12$ GeV and $E = 12$ keVee, and 0.58×10^{-5} events/kg/day/keVee for $m = 15$ GeV and $E = 15$ keVee. Because the minimum WIMP speeds v_q are large in these examples, a smaller velocity dispersion of the WIMP distribution leads to smaller rates (since a smaller amount of WIMPs have velocities larger than v_q). So the signal rate difference $R_{s-\max} - R_{s-\min}$ is even smaller for smaller values of σ_v.

The left-bottom panel of Fig. 5 shows the signal rate as function of UT for $m = 10$ GeV and $V_{\rm lab} = 288.3$ km/s for several energies between 2 keVee and 12 keVee. The rate decreases but A_s increases with increasing energy and the best conditions for observability happen at some energy where neither the rate nor A_s are very small. The rates for low energies between 2 keVee and 6 keVee are dominated by the usual (i.e. non-channeled) rate and the daily modulation is due purely to the change in WIMP kinetic energy in the lab frame as the Earth rotates around itself. The rates for energies above 8 keVee (green/gray lines) are purely due to channeling, i.e. the usual rate is zero. For intermediate energies, 6 keVee to 8 keVee, the usual and channeled rates both contribute and thus the daily modulation is due to both the channeling effect and the daily change in the usual rate. For $E = 2$, 4, 6, 8, 10 and 12 keVee, the values of $R_{s-\max} - R_{s-\min}$ given in events/kg/day/keVee are respectively 4.3×10^{-4}, 0.5×10^{-3}, 0.92×10^{-3}, 2.8×10^{-4}, 0.77×10^{-3} and 0.52×10^{-3}. Notice that for all the energies shown the difference in rate is similar, but the largest A_s values happen at energies above 8 keVee, for which the rate is only due to channeling. The channeling daily modulation amplitude increases as the ratio of the velocity dispersion to the average speed of the WIMPs that contribute to the signal (i.e. with $v > v_q$) decreases. This ratio is small and thus A_s large for large values of v_q. Notice that the phase of the modulation due to channeling depends on the orientation of the crystal with respect to the Galaxy and the phase of the modulation in the usual rate does not, which would allow to distinguish both effects, if they were observable. The case of $m = 10$ GeV and $E = 6$ keVee has the largest rate difference, but is not observable at 3σ according to Eq. 32 (not even at the 1σ level).

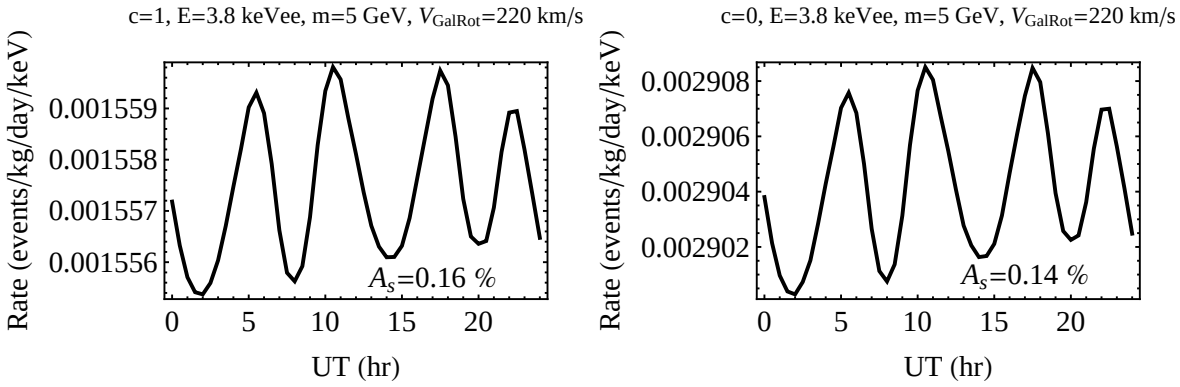

FIG. 6: Signal rate as function of UT during 24 hours for $E = 3.8$ keVee and $m = 5$ GeV, with $V_{\rm lab} = 228.4$ km/s, $\sigma_v = 300$ km/s, $\sigma_p = 2 \times 10^{-40}{\rm cm}^2$, and $Q_{\rm Na} = 0.2$, $Q_{\rm I} = 0.09$ for (a) $c = 1$ and (b) $c = 0$. The daily modulation is not observable in both cases.

Choosing $\sigma_p = 4 \times 10^{-40}{\rm cm}^2$ (still within the DAMA allowed region but not compatible with the recent XENON100 result) results in a rate difference of 1.84×10^{-3} events/kg/day/keVee for this case which would not be observable even at the 1σ level.

Finally, we would like to compare our results with those obtained in Ref. [3] by Creswick *et al.* They found a relative daily modulation amplitude A_s =0.85% (their definition of amplitude differs by a factor of 2 from ours, so they quote 1.7%) for 5 GeV WIMP mass and 3.8 keVee measured energy (in which case $v_q = 471.2$ km/s and 936.6 km/s for channeled Na and I recoils, respectively. There are no WIMPs with the speed required for I recoils, thus only Na recoils are possible). In order to compare our calculation with theirs, we compute the signal event rate as function of time for $c = 1$, $T = 293$ K (temperature corrections are not included in the calculation of Creswick *et al.*) and choosing all the other parameters very close to those used in Ref. [3], i.e. $V_{\rm lab} = 228.4$ km/s and $\sigma_v = 300$ km/s. A WIMP mass of 5 GeV is outside the region of parameter space compatible with the annual modulation reported by DAMA [17]. Since A_s does not depend on σ_p, we choose an arbitrary value of $\sigma_p = 2 \times 10^{-40}{\rm cm}^2$ to plot the signal rate as a function of UT (the upper bound given by TEXONO and CoGeNT [20] is five times larger, $\sigma_p < 1 \times 10^{-39}{\rm cm}^2$). Our result is shown in Fig. 6.a. We find A_s =0.16% ($R_{s-\rm max} - R_{s-\rm min} = 4.4 \times 10^{-6}$ events/kg/day/keVee). Even when we consider the extreme choice of $c = 0$ to compute temperature effects (an unrealistic value for which the channeling fractions are larger) with the same parameters, we get $A_s = 0.14\%$. This case is shown in Fig. 6.b.

C. Future Prospects for DAMA and other Experiments

The daily modulation might be detectable in other experiments with smaller background or WIMP halo components with a smaller dispersion such as streams or a thick disk. The amplitude of the daily modulation increases as the WIMP velocity distribution is narrower i.e. for larger values of the average velocity and smaller values of the velocity dispersion of the detectable WIMPs (which is not σ_v), i.e. those with velocity larger than v_q. This is easy to understand since as the dispersion increases more channels are available for channeling of the recoiling ions. In the limit in which the velocity distribution would be isotropic with respect to the detector, the daily rotation would not introduce any difference in the rate due to channeling. Having a large relative signal modulation amplitude A_s is not sufficient for observability. In Eq. 32 what is important is $(A_s\ R_s) = (R_{s-\max} - R_{s-\min})/2$. However, the condition in Eq. 32 was derived considering the total rate in the DAMA experiment, which is dominated by background. For an experiment where the background is negligible, i.e. $R_T = R_s + R_b \simeq R_s$, we can derive a different observability condition (at the 3σ level) from Eq. 29,

$$R_s\ A_s^2 = A_s\ (R_{s-\max} - R_{s-\min})/2 > 9/(2MT\ \Delta E). \tag{33}$$

This condition might be easier to satisfy in future experiments.

One could ask which is the maximum level of total rate with the current DAMA exposure that would be needed to make the signal daily modulation observable. Inserting the current exposure of DAMA (1.17 ton year) in Eq. 29, we have

$$(A_s\ R_s)^2/R_T > 1.05 \times 10^{-5}\ \text{events/kg/day/keVee}, \tag{34}$$

which using $A_s R_s = (R_{s-\max} - R_{s-\min})/2$, becomes

$$R_T < \frac{(R_{s-\max} - R_{s-\min})^2}{4.2 \times 10^{-5}\ \text{events/kg/day/keVee}}. \tag{35}$$

Even in the case with the highest rate difference we found, i.e. $R_{s-\max} - R_{s-\min} = 0.98 \times 10^{-3}$ events/kg/day/keVee (the $m = 10$ GeV, $E = 6$ keVee, $V_{\rm lab} = 288.3$ km/s example shown in the bottom-left panel of Fig. 5) observability would require

$$R_T < 0.023\ \text{events/kg/day/keVee}, \tag{36}$$

roughly 1/40 of what is now.

We could ask instead what exposure would be needed with the current total rate in the DAMA experiment to make the daily modulation observable. Setting $R_T \simeq 1$ events/kg/day/keVee in Eq. 29, we obtain

$$\frac{MT\Delta E}{(\text{events/kg/day/keVee})} > \frac{9}{2\left(A_s\ R_s\right)^2} = \frac{18}{\left(R_{s-\max} - R_{s-\min}\right)^2}. \tag{37}$$

Again, for the case with the highest rate difference we found ($m = 10$ GeV, $E = 6$ keVee and $V_{\rm lab} = 288.3$ km/s) and with $\Delta E \simeq 1$ keVee we would require an exposure 40 times larger,

$$MT > 51.3 \text{ ton year}. \tag{38}$$

We have computed the daily modulation due to channeling in other material such as Ge, solid Xe and solid Ne, and we find that it will be very difficult to observe. For light WIMPs the cross section can be larger than for heavier ones without violating experimental bounds, $\sigma_p = 10^{-39}\text{cm}^2$ [20] and this favors the detection of the daily modulation. We find that for a WIMP mass $m = 5$ GeV the daily modulation due to channeling may be observable in solid Ne if the signal would be above threshold and assuming no background. The geometric channeling fraction reaches a maximum at around 10 keV for solid Ne [6], thus the largest modulation amplitude happens at that energy. For example for a solid Ne detector operating at 23 K at Gran Sasso, for $E = 10$ keV, assuming $Q_{\rm Ne} = 0.25$ [21], $c = 1$ and with velocity distribution parameters $\sigma_v = 300$ km/s and $V_{\rm lab} = 228.4$ km/s we find $R_s A_s^2 = 3.68 \times 10^{-5}$ events/kg/day/keVee. Using Eq. 33 we find that the exposure needed to observe this modulation at 3σ is $MT = 0.33$ ton year. For the same parameters but for $m = 7$ GeV and $\sigma_p = 2 \times 10^{-40}\text{cm}^2$ (parameters compatible with the possible dark matter signal found by CoGeNT and with DAMA according to Ref. [22]), we find $R_s A_s^2 = 7.2 \times 10^{-7}$ events/kg/day/keVee, and the exposure needed is $MT = 17.1$ ton year. The usual rate is zero in both cases, and the modulation is just due to channeling. The signal rate during 24 hours and the required exposures for the two cases are shown in Fig. 7 and Table I, respectively.

We intend to further explore the observability of a daily modulation in future experiments for different halo models in future work.

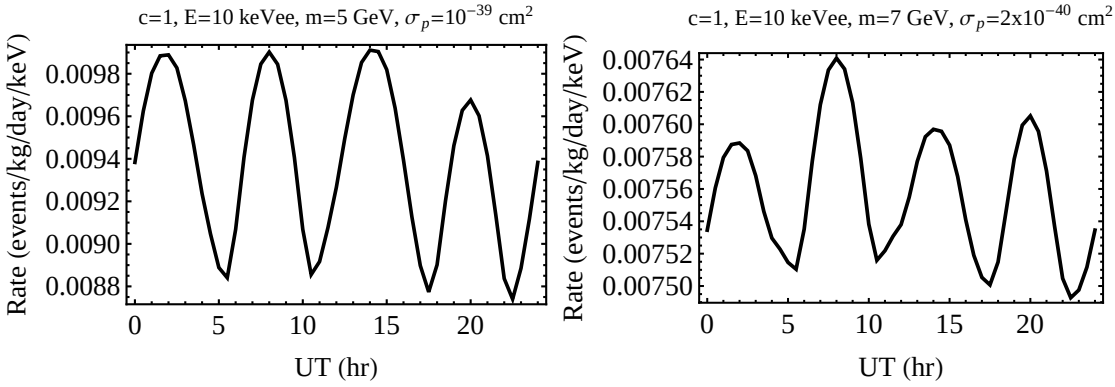

FIG. 7: Signal rate as function of UT during 24 hours for a solid Ne detector operating at $T = 23$ K at Gran Sasso for $E = 10$ keVee, $Q = 0.25$, $c = 1$, $\sigma_v = 300$ km/s, $V_{\rm lab} = 228.4$ km/s and for (a) $m = 5$ GeV and $\sigma_p = 10^{-39}$cm^2, and (b) $m = 7$ GeV and $\sigma_p = 2 \times 10^{-40}$cm^2.

TABLE I: Observability in solid Ne detector

Case	σ_p (cm^2)	MT (ton year)
$m = 5$ GeV	10^{-39}	0.33
$m = 7$ GeV	2×10^{-40}	17.1

Acknowledgments

G.G. and N.B. were supported in part by the US Department of Energy Grant DE-FG03-91ER40662, Task C. P.G. was supported in part by the NFS grant PHY-0756962 at the University of Utah.

Appendix A: Crystal Orientation

We need to orient the crystal with respect to the laboratory. We define a reference frame fixed with the laboratory and orient its axes so that the xy plane is horizontal, the x-axis points North, the y-axis points West, and the z-axis points to the zenith. We denote its unit coordinate vectors as $\hat{\mathcal{N}}$, $\hat{\mathcal{W}}$ and $\hat{\mathcal{Z}}$, respectively. We also define the crystal frame with X, Y, Z cartesian axes fixed with the crystal. The unit coordinate vectors of the crystal frame are $\hat{\mathbf{X}}$, $\hat{\mathbf{Y}}$ and $\hat{\mathbf{Z}}$.

We now want to connect the laboratory frame to the crystal frame. Let the standard

orientation correspond to the configuration in which $\hat{\mathbf{X}} = \hat{\mathcal{N}}$, $\hat{\mathbf{Y}} = \hat{\mathcal{W}}$, and $\hat{\mathbf{Z}} = \hat{\mathcal{Z}}$. We start with the crystal in the standard orientation, and we turn it into any other orientation $\hat{\mathbf{X}}$, $\hat{\mathbf{Y}}$, $\hat{\mathbf{Z}}$. In this new orientation, each of the unit coordinate vectors of the crystal frame can be written in terms of unit coordinate vectors of the lab frame,

$$\begin{aligned}
\hat{\mathbf{X}} &= \alpha_X\, \hat{\mathcal{N}} + \beta_X\, \hat{\mathcal{W}} + \gamma_X\, \hat{\mathcal{Z}}, \\
\hat{\mathbf{Y}} &= \alpha_Y\, \hat{\mathcal{N}} + \beta_Y\, \hat{\mathcal{W}} + \gamma_Y\, \hat{\mathcal{Z}}, \\
\hat{\mathbf{Z}} &= \alpha_Z\, \hat{\mathcal{N}} + \beta_Z\, \hat{\mathcal{W}} + \gamma_Z\, \hat{\mathcal{Z}},
\end{aligned} \tag{A1}$$

where α_i, β_i and γ_i are the "direction cosines" between the two sets of cartesian coordinates of the lab and crystal frames, for $i = X, Y, Z$. For example, the coordinate vector $\hat{\mathbf{X}}$ of the crystal has a particular angle with each of the lab frame coordinate vectors $\hat{\mathcal{N}}$, $\hat{\mathcal{W}}$, $\hat{\mathcal{Z}}$. Let a_X be the angle between $\hat{\mathbf{X}}$ and $\hat{\mathcal{N}}$, b_X the angle between $\hat{\mathbf{X}}$ and $\hat{\mathcal{W}}$, and c_X the angle between $\hat{\mathbf{X}}$ and $\hat{\mathcal{Z}}$. The direction cosines of the unit vector $\hat{\mathbf{X}}$ are given by,

$$\begin{aligned}
\alpha_X &\equiv \cos a_X = \hat{\mathbf{X}} \cdot \hat{\mathcal{N}}, \\
\beta_X &\equiv \cos b_X = \hat{\mathbf{X}} \cdot \hat{\mathcal{W}}, \\
\gamma_X &\equiv \cos c_X = \hat{\mathbf{X}} \cdot \hat{\mathcal{Z}}.
\end{aligned} \tag{A2}$$

We can find the direction cosines for $\hat{\mathbf{Y}}$ and $\hat{\mathbf{Z}}$ unit vectors in a similar way. From these definitions it follows that $\alpha_i\ \alpha_j + \beta_i\ \beta_j + \gamma_i\ \gamma_j = \delta_{ij}$ where $i, j = X, Y, Z$. We prefer using direction cosines over Euler angles because the direction cosines can easily be measured for any known orientation of a crystal in a laboratory, whereas it may be difficult to specify the Euler angles.

Eq. A1 gives the transformation from the lab frame to the crystal frame. We can also find the lab coordinate vectors in terms of the crystal coordinate vectors,

$$\begin{aligned}
\hat{\mathcal{N}} &= \alpha_X\, \hat{\mathbf{X}} + \alpha_Y\, \hat{\mathbf{Y}} + \alpha_Z\, \hat{\mathbf{Z}}, \\
\hat{\mathcal{W}} &= \beta_X\, \hat{\mathbf{X}} + \beta_Y\, \hat{\mathbf{Y}} + \beta_Z\, \hat{\mathbf{Z}}, \\
\hat{\mathcal{Z}} &= \gamma_X\, \hat{\mathbf{X}} + \gamma_Y\, \hat{\mathbf{Y}} + \gamma_Z\, \hat{\mathbf{Z}}.
\end{aligned} \tag{A3}$$

In the results we show in this paper, we took $\alpha_X = \beta_Y = \gamma_Z = 1$ and all the other α_i, β_i and γ_i equal to zero. Choosing a different orientation for the crystal does not change the average rate, but A_s may change by a factor of 2 for NaI depending on the orientation of the crystal. The observability condition is still not satisfied.

1. Lab to equatorial transformation

To connect the laboratory frame to the equatorial coordinate frame, we recall the definition of the geocentric equatorial inertial (GEI) frame: its origin is at the center of the Earth, its x_e-axis points in the direction of the vernal equinox, its y_e-axis points to the point on the celestial equator with right ascension 90° (so that the cartesian frame is right-handed), and its z_e-axis points to the north celestial pole. We denote its unit coordinate vectors as $\hat{\mathbf{x}}_e$, $\hat{\mathbf{y}}_e$, and $\hat{\mathbf{z}}_e$. We want to find the transformation formulas from the laboratory frame to the GEI frame.

This transformation can be achieved by two successive rotations. The first rotation is by an angle of $(90^\circ - \lambda_{\rm lab})$ counterclockwise about the laboratory y-axis to align the new $x'y'$ plane with the plane of the celestial equator. Here $\lambda_{\rm lab}$ is the latitude of the laboratory in degrees, with northern latitudes taken as positive and southern latitudes taken as negative. With this rotation, the new z'-axis points to the north celestial pole. The second rotation is by an angle $(15t_{\rm lab} + 180)$ degrees clockwise about the new z'-axis to bring the x'-axis in the direction of the vernal equinox. Here $t_{\rm lab}$ is the laboratory Local Apparent Sidereal Time (LAST) in hours (the LAST is the hour angle of the vernal equinox at the location of the laboratory). One has

$$t_{\rm lab} = t_{\rm GAST} + l_{\rm lab}/15, \tag{A4}$$

where $t_{\rm GAST}$ is the Greenwich Apparent Sidereal Time (GAST) in hours and $l_{\rm lab}$ is the longitude in degrees measured positive in the eastward direction (e.g. $l_{\rm lab} = +110^\circ$ for 110° E and $l_{\rm lab} = -110^\circ$ for 110° W).

The current local apparent sidereal time for any specified longitude $l_{\rm lab}$ can be computed online, for example on the website of the US Naval Observatory at http://tycho.usno.navy.mil/ sidereal.html (accessed Sept 19, 2010). As an alternative, one can use the following formula [23, 24] for the Greenwich mean sidereal time (which differs from the Greenwich apparent sidereal time by less than 1.2 seconds, completely negligible for our purposes),

$$t_{\rm GAST} = (101.0308 + 36000.770\, T_0 + 15.04107\, {\rm UT})/15, \tag{A5}$$

where

$$T_0 = \frac{\lfloor {\rm MJD} \rfloor - 55197.5}{36525.0}. \tag{A6}$$

Here UT is the Universal Time in hours, $\lfloor \mathrm{MJD} \rfloor$ is the integer part of the modified Julian date (MJD), which is the time measured in days from 00:00 UT on 17 November 1858 (Julian date 2400000.5). Note that T_0 is the time in Julian centuries (36525 days) from 12:00 UT on 1 January 2010 to the previous midnight. At 12:00 UT on 1 January 2010, the Julian date is 2455198, and the MJD is 55197.5. Also the the 15.04107/15 in Eq. A5 corrects from solar time (UT) to sidereal time. Sidereal day is shorter than Solar day by 3.9 minutes. In this paper, all our results are computed for the particular arbitrary day of 25 September 2010, for which $T_0 = 0.00729637$.

Note also that UT is different from coordinated Universal Time (UTC) which is the time scale usually used for data recording. UTC is atomic time adjusted by an integral number of seconds to keep it within 0.6 s of UT. For our purposes the difference between UT and UTC is negligible.

Taking into account the two rotations explained above, one can find the transformation equations of the unit vectors,

$$\begin{aligned}
\hat{\mathbf{x}}_e &= -\cos(t^\circ_{\rm lab}) \left[\sin(\lambda_{\rm lab})\hat{\mathcal{N}} - \cos(\lambda_{\rm lab})\hat{\mathcal{Z}}\right] + \sin(t^\circ_{\rm lab})\hat{\mathcal{W}}, \\
\hat{\mathbf{y}}_e &= -\sin(t^\circ_{\rm lab}) \left[\sin(\lambda_{\rm lab})\hat{\mathcal{N}} - \cos(\lambda_{\rm lab})\hat{\mathcal{Z}}\right] - \cos(t^\circ_{\rm lab})\hat{\mathcal{W}}, \\
\hat{\mathbf{z}}_e &= \cos(\lambda_{\rm lab})\hat{\mathcal{N}} + \sin(\lambda_{\rm lab})\hat{\mathcal{Z}},
\end{aligned} \tag{A7}$$

where $t^\circ_{\rm lab} = 15 t_{\rm lab}$ is the laboratory LAST converted to degrees.

As a check, for a laboratory on the equator at local sidereal time 0, i.e. $\lambda_{\rm lab} = 0^\circ$ and $t^\circ_{\rm lab} = 0^\circ$, one has $\hat{\mathbf{x}}_e = \hat{\mathcal{Z}}$, $\hat{\mathbf{y}}_e = -\hat{\mathcal{W}}$, and $\hat{\mathbf{z}}_e = \hat{\mathcal{N}}$; six sidereal hours later at the same laboratory, i.e. $\lambda_{\rm lab} = 0^\circ$ and $t^\circ_{\rm lab} = 90^\circ$, one has $\hat{\mathbf{x}}_e = \hat{\mathcal{W}}$, $\hat{\mathbf{y}}_e = \hat{\mathcal{Z}}$, and $\hat{\mathbf{z}}_e = \hat{\mathcal{N}}$; for a laboratory at the South Pole ($\lambda_{\rm lab} = -90^\circ$), using the direction of the Greenwich meridian in place of the "North" axis $\hat{\mathcal{N}}$ so that the local sidereal time at the South Pole by convention coincides with the Greenwich sidereal time, one has $\hat{\mathbf{x}}_e = \hat{\mathcal{N}}$, $\hat{\mathbf{y}}_e = -\hat{\mathcal{W}}$, and $\hat{\mathbf{z}}_e = -\hat{\mathcal{Z}}$ at $t^\circ_{\rm lab} = 0^\circ$ and $\hat{\mathbf{x}}_e = \hat{\mathcal{W}}$, $\hat{\mathbf{y}}_e = \hat{\mathcal{N}}$, and $\hat{\mathbf{z}}_e = -\hat{\mathcal{Z}}$ at $t^\circ_{\rm lab} = 90^\circ$. All of these are correctly given by Eq. A7.

The formulas in Eq. A7 can be inverted, and the transformation from the equatorial

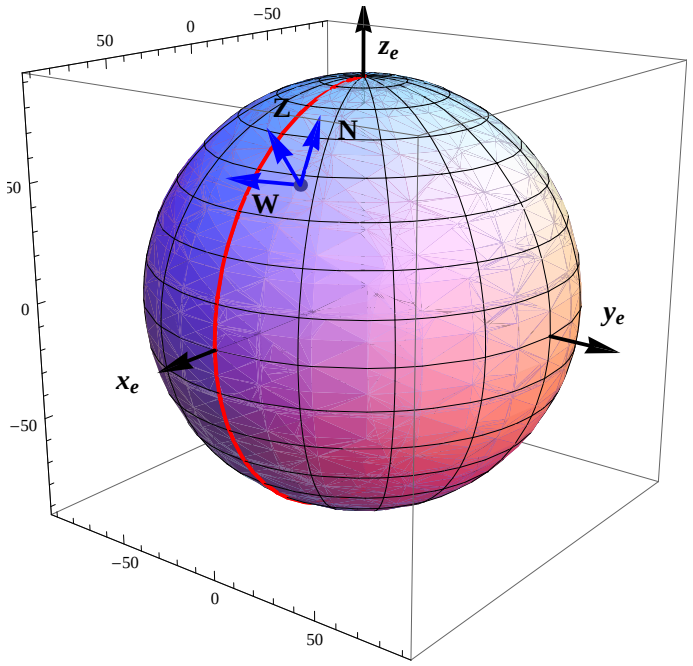

FIG. 8: (Color online) Earth's sphere in the equatorial frame ($\hat{\mathbf{x}}_e$,$\hat{\mathbf{y}}_e$,$\hat{\mathbf{z}}_e$) specified with black arrows. The laboratory frame (N,W,Z) specified with blue/dark gray arrows is also shown.

frame to the lab frame is achieved:

$$\begin{aligned}
\hat{\mathcal{N}} &= -\sin(\lambda_{\rm lab})\,[\cos(t^{\circ}_{\rm lab})\hat{\mathbf{x}}_e + \sin(t^{\circ}_{\rm lab})\hat{\mathbf{y}}_e] + \cos(\lambda_{\rm lab})\hat{\mathbf{z}}_e,\\
\hat{\mathcal{W}} &= \sin(t^{\circ}_{\rm lab})\hat{\mathbf{x}}_e - \cos(t^{\circ}_{\rm lab})\ \hat{\mathbf{y}}_e,\\
\hat{\mathcal{Z}} &= \cos(\lambda_{\rm lab})\,[\cos(t^{\circ}_{\rm lab})\hat{\mathbf{x}}_e + \sin(t^{\circ}_{\rm lab})\hat{\mathbf{y}}_e] + \sin(\lambda_{\rm lab})\hat{\mathbf{z}}_e. \qquad \text{(A8)}
\end{aligned}$$

The latitude and longitude of Gran Sasso are $\lambda_{\rm lab} = 42.45^{\circ}$ and $l_{\rm lab} = 13.7^{\circ}$, respectively.

Fig. 8 shows the laboratory frame ($\hat{\mathcal{N}}$, $\hat{\mathcal{W}}$, $\hat{\mathcal{Z}}$) and the equatorial coordinate frame ($\hat{\mathbf{x}}_e$,$\hat{\mathbf{y}}_e$,$\hat{\mathbf{z}}_e$) plotted on the Earth's sphere at $UT = 0$ using Eq. A8.

2. Equatorial to galactic transformation

To connect the equatorial frame to the galactic coordinate frame, we recall the definition of the galactic coordinate system: its origin is at the position of the Sun, its x_g-axis points towards the galactic center, its y_g-axis points in the direction of the galactic rotation, and its z_g-axis points to the north galactic pole.

For the epoch of January 1950.0 the transformation from the equatorial frame ($\hat{\mathbf{x}}_e, \hat{\mathbf{y}}_e, \hat{\mathbf{z}}_e$)

to the galactic frame $(\hat{\mathbf{x}}_g, \hat{\mathbf{y}}_g, \hat{\mathbf{z}}_g)$ is given by [25]:

$$\begin{aligned}
\hat{\mathbf{x}}_g &= \hat{\mathbf{x}}_e\ (-0.06699) + \hat{\mathbf{y}}_e\ (-0.8728) + \hat{\mathbf{z}}_e\ (-0.4835), \\
\hat{\mathbf{y}}_g &= \hat{\mathbf{x}}_e\ (0.4927) + \hat{\mathbf{y}}_e\ (-0.4503) + \hat{\mathbf{z}}_e\ (0.7446), \\
\hat{\mathbf{z}}_g &= \hat{\mathbf{x}}_e\ (-0.8676) + \hat{\mathbf{y}}_e\ (-0.1883) + \hat{\mathbf{z}}_e\ (0.4602).
\end{aligned} \tag{A9}$$

The transformation from the galactic frame to the equatorial frame is given by

$$\begin{aligned}
\hat{\mathbf{x}}_e &= \hat{\mathbf{x}}_g\ (-0.06699) + \hat{\mathbf{y}}_g\ (0.4927) + \hat{\mathbf{z}}_g\ (-0.8676), \\
\hat{\mathbf{y}}_e &= \hat{\mathbf{x}}_g\ (-0.8728) + \hat{\mathbf{y}}_g\ (-0.4503) + \hat{\mathbf{z}}_g\ (-0.1884), \\
\hat{\mathbf{z}}_e &= \hat{\mathbf{x}}_g\ (-0.4835) + \hat{\mathbf{y}}_g\ (0.7446) + \hat{\mathbf{z}}_g\ (0.4602).
\end{aligned} \tag{A10}$$

The change of Eqs. A9 and A10 from the epoch of January 1950.0 to 25 September 2010 is small and would not affect the final results in this paper.

Appendix B: Laboratory motion

The velocity of the lab with respect to the center of the Galaxy can be divided into four components (as in Eq. 9): $\mathbf{V}_{\rm GalRot}$, $\mathbf{V}_{\rm Solar}$, $\mathbf{V}_{\rm EarthRev}$ and $\mathbf{V}_{\rm EarthRot}$.

We take $V_{\rm GalRot} = 220$ km/s or 280 km/s [12], $V_{\rm Solar} = 18$ km/s [26], $V_{\rm EarthRev} = 29.8$ km/s and $V_{\rm EarthRot} = (0.465102\ {\rm km/s}) \cos\lambda_{\rm lab}$, where $\lambda_{\rm lab}$ is the latitude of the lab. Values of $V_{\rm GalRot} = 220$ km/s or 280 km/s results in $V_{\rm lab} = 228.4$ km/s or 288.3 km/s, respectively (see Appendix B.5 for the equation of $\mathbf{V}_{\rm lab}$). Thus, $\mathbf{V}_{\rm lab}$ is dominated by the galactic rotation velocity.

We need to compute $\hat{\mathbf{q}} \cdot \mathbf{V}_{\rm lab}$, where $\hat{\mathbf{q}}$ is given in the crystal reference frame ($\hat{\mathbf{q}} = q_X\ \hat{\mathbf{X}} + q_Y\ \hat{\mathbf{Y}} + q_Z\ \hat{\mathbf{Z}}$). Therefore, we need to also write $\mathbf{V}_{\rm lab}$ in the crystal frame. We have,

$$\hat{\mathbf{q}} \cdot \mathbf{V}_{\rm lab} = \hat{\mathbf{q}} \cdot \mathbf{V}_{\rm GalRot} + \hat{\mathbf{q}} \cdot \mathbf{V}_{\rm Solar} + \hat{\mathbf{q}} \cdot \mathbf{V}_{\rm EarthRev} + \hat{\mathbf{q}} \cdot \mathbf{V}_{\rm EarthRot}. \tag{B1}$$

We will compute each term on the right-hand side of Eq. B1 individually.

1. Galactic rotation

The velocity of the galactic rotation $\mathbf{V}_{\rm GalRot}$ is defined in the galactic reference frame,

$$\mathbf{V}_{\rm GalRot} = V_{\rm GalRot} \hat{\mathbf{y}}_g, \tag{B2}$$

where $V_{\rm GalRot}$ is the galactic rotation speed (i.e. the local circular speed), and $\hat{\mathbf{y}}_g$ is in the direction of the galactic rotation. Following Ref. [12] , we take $V_{\rm GalRot} = 220$ km/s or 280 km/s. Using the conversions in Eq. A9, we can write $\hat{\mathbf{y}}_g$ in the equatorial reference frame in terms of ($\hat{\mathbf{x}}_e$,$\hat{\mathbf{y}}_e$,$\hat{\mathbf{z}}_e$). Then, we use Eq. A7 to transform from the equatorial frame to the lab frame ($\hat{\mathcal{N}}, \hat{\mathcal{W}}, \hat{\mathcal{Z}}$), and finally we use Eq. A3 to transform from the lab frame to the crystal frame ($\hat{\mathbf{X}}, \hat{\mathbf{Y}}, \hat{\mathbf{Z}}$).

Thus, we can use Eq. A3 to write $\mathbf{V}_{\rm GalRot}$ in terms of the crystal frame coordinates, and compute $\hat{\mathbf{q}} \cdot \mathbf{V}_{\rm GalRot}$,

$$\hat{\mathbf{q}} \cdot \mathbf{V}_{\rm GalRot} = q_X V_{\rm GalRot,X} + q_Y V_{\rm GalRot,Y} + q_Z V_{\rm GalRot,Z}. \tag{B3}$$

We have

$$\begin{aligned}\hat{\mathbf{q}} \cdot \mathbf{V}_{\rm GalRot} = V_{\rm GalRot}\Bigg\{ &\Bigg([-0.4927\cos(t^\circ_{\rm lab}) + 0.4503\sin(t^\circ_{\rm lab})]\sin(\lambda_{\rm lab}) + 0.7446\cos(\lambda_{\rm lab})\Bigg) \\ &(\alpha_X q_X + \alpha_Y q_Y + \alpha_Z q_Z) + \Bigg(0.4927\sin(t^\circ_{\rm lab}) + 0.4503\cos(t^\circ_{\rm lab})\Bigg)(\beta_X q_X + \beta_Y q_Y + \beta_Z q_Z) \\ &+ \Bigg([0.4927\cos(t^\circ_{\rm lab}) - 0.4503\sin(t^\circ_{\rm lab})]\cos(\lambda_{\rm lab}) + 0.7446\sin(\lambda_{\rm lab})\Bigg) \\ &(\gamma_X q_X + \gamma_Y q_Y + \gamma_Z q_Z)\Bigg\}. \end{aligned} \tag{B4}$$

Eq. B4 has a time dependence through $t^\circ_{\rm lab}$ and would be responsible for any daily modulation in the rate.

2. Solar motion

The velocity of the Sun's motion in the galactic rest frame is,

$$\mathbf{V}_{\rm Solar} = U\hat{\mathbf{x}}_g + V\hat{\mathbf{y}}_g + W\hat{\mathbf{z}}_g, \tag{B5}$$

where $(U, V, W)_\odot = (11.1, 12.2, 7.3)$ km/s [26]. Using Eq. A9, we can transform from the galactic frame to the equatorial frame, and using Eq. A7 we can transform from the equatorial frame to the lab frame. Then we can use Eq. A3 to write $\mathbf{V}_{\rm Solar}$ in terms of the crystal frame coordinates.

Thus, we can compute $\hat{\mathbf{q}} \cdot \mathbf{V}_{\rm Solar}$ as

$$\begin{aligned}\hat{\mathbf{q}} \cdot \mathbf{V}_{\rm Solar} = &\Big(\big[(1.066 \text{ km/s}) \cos(t^\circ_{\rm lab}) + (16.56 \text{ km/s}) \sin(t^\circ_{\rm lab})\big] \sin(\lambda_{\rm lab}) + (7.077 \text{ km/s}) \cos(\lambda_{\rm lab}) \Big) \\ &(\alpha_X q_X + \alpha_Y q_Y + \alpha_Z q_Z) + \Big(- (1.066 \text{ km/s}) \sin(t^\circ_{\rm lab}) + (16.56 \text{ km/s}) \cos(t^\circ_{\rm lab}) \Big) \\ &(\beta_X q_X + \beta_Y q_Y + \beta_Z q_Z) + \Big(- \big[(1.066 \text{ km/s}) \cos(t^\circ_{\rm lab}) + (16.56 \text{ km/s}) \sin(t^\circ_{\rm lab})\big] \cos(\lambda_{\rm lab}) \\ &+ (7.077 \text{ km/s}) \sin(\lambda_{\rm lab}) \Big) (\gamma_X q_X + \gamma_Y q_Y + \gamma_Z q_Z). \end{aligned} \tag{B6}$$

Clearly, Eq. B6 has a time dependence through $t^\circ_{\rm lab}$ and would be responsible of any daily modulation in the rate.

3. Earth's revolution

The velocity of the Earth's revolution around the sun is given in terms of the Sun ecliptic longitude $\lambda(t)$ as [28]

$$\begin{aligned}\mathbf{V}_{\rm EarthRev} = &V_\oplus(\lambda(t))[\cos\beta(x)\sin(\lambda(t)-\lambda_x)\hat{\mathbf{x}}_g \\ &+ \cos\beta(y)\sin(\lambda(t)-\lambda_y)\hat{\mathbf{y}}_g + \cos\beta(z)\sin(\lambda(t)-\lambda_z)\hat{\mathbf{z}}_g], \end{aligned} \tag{B7}$$

where $V_\oplus = 29.8$ km/s is the orbital speed of the Earth, $V_\oplus(\lambda(t)) = V_\oplus[1 - e\sin(\lambda(t) - \lambda_0)]$, $e = 0.016722$, and $\lambda_0 = 13^\circ + 1^\circ$ are the ellipticity of the Earth's orbit and the ecliptic longitude of the orbit's minor axis, respectively, and $\beta_i = (-5^\circ.5303, 59^\circ.575, 29^\circ.812)$ and $\lambda_i = (266^\circ.141, -13^\circ.3485, 179^\circ.3212)$ are the ecliptic latitudes and longitudes of the ($\hat{\mathbf{x}}_g$,$\hat{\mathbf{y}}_g$,$\hat{\mathbf{z}}_g$) axes, respectively.

The Sun's ecliptic longitude $\lambda(t)$ can be expressed as (p. 77 of Ref. [27] and Ref. [28]),

$$\lambda(t) = L + (1^\circ.915 - 0^\circ.0048 T_0)\sin g + 0^\circ.020 \sin 2g, \tag{B8}$$

where $L = 281^\circ.0298 + 36000^\circ.77 T_0 + 0^\circ.04107 UT$ is the mean longitude of the Sun corrected for aberration, $g = 357^\circ.9258 + 35999^\circ.05 T_0 + 0^\circ.04107 UT$ is the mean anomaly (polar angle of orbit).

Using Eq. A9, we can transform from the galactic frame to the equatorial frame, and using Eq. A7 we can transform from the equatorial frame to the lab frame $(\hat{\mathcal{N}}, \hat{\mathcal{W}}, \hat{\mathcal{Z}})$. Then we can use Eq. A3 to write $\mathbf{V}_{\rm Solar}$ in terms of the crystal frame coordinates.

Thus, we can compute $\hat{\mathbf{q}} \cdot \mathbf{V}_{\rm EarthRev}$ as

$$\begin{aligned}\hat{\mathbf{q}} \cdot \mathbf{V}_{\rm EarthRev} = V_{\oplus}(\lambda(t))\Big\{ &\big[-\cos(t^{\circ}_{\rm lab})\sin(\lambda_{\rm lab})\mathcal{A}(t) - \sin(t^{\circ}_{\rm lab})\sin(\lambda_{\rm lab})\mathcal{B}(t) + \cos(\lambda_{\rm lab})\mathcal{C}(t)\big] \\ &(\alpha_X q_X + \alpha_Y q_Y + \alpha_Z q_Z) + \big[\sin(t^{\circ}_{\rm lab})\mathcal{A}(t) - \cos(t^{\circ}_{\rm lab})\mathcal{B}(t)\big]\,(\beta_X q_X + \beta_Y q_Y + \beta_Z q_Z) \\ &+ \big[\cos(t^{\circ}_{\rm lab})\cos(\lambda_{\rm lab})\mathcal{A}(t) + \sin(t^{\circ}_{\rm lab})\cos(\lambda_{\rm lab})\mathcal{B}(t) + \sin(\lambda_{\rm lab})\mathcal{C}(t)\big]\,(\gamma_X q_X + \gamma_Y q_Y + \gamma_Z q_Z)\Big\},\end{aligned} \tag{B9}$$

where

$$\begin{aligned}\mathcal{A}(t) &= (-0.06699)\cos\beta(x)\sin(\lambda(t) - \lambda_x) + (0.4927)\cos\beta(y)\sin(\lambda(t) - \lambda_y) \\ &\quad + (-0.8676)\cos\beta(z)\sin(\lambda(t) - \lambda_z), \\ \mathcal{B}(t) &= (-0.8728)\cos\beta(x)\sin(\lambda(t) - \lambda_x) + (-0.4503)\cos\beta(y)\sin(\lambda(t) - \lambda_y) \\ &\quad + (-0.1883)\cos\beta(z)\sin(\lambda(t) - \lambda_z), \\ \mathcal{C}(t) &= (-0.4835)\cos\beta(x)\sin(\lambda(t) - \lambda_x) + (0.7446)\cos\beta(y)\sin(\lambda(t) - \lambda_y) \\ &\quad + (0.4602)\cos\beta(z)\sin(\lambda(t) - \lambda_z).\end{aligned} \tag{B10}$$

Eq. B9 has a time dependence through $t^{\circ}_{\rm lab}$ and $\lambda(t)$ and would be responsible for any daily modulation in the rate.

4. Earth's rotation

Finally, we want to compute $\mathbf{V}_{\rm EarthRot}$, the velocity of Earth's rotation around itself. We have

$$\mathbf{V}_{\rm EarthRot} = -V_{\rm RotEq}\cos\lambda_{\rm lab}\hat{\mathcal{W}}, \tag{B11}$$

where $V_{\rm RotEq}$ is the Earth's rotation speed at the equator, and is defined as $V_{\rm RotEq} = 2\pi R_{\oplus}/(1\text{ sidereal day})$. The Earth's equatorial radius is $R_{\oplus} = 6378.137$ km, and one sidereal day is 23.9344696 hr= 86164 s. therefore $V_{\rm RotEq} = 0.465102$ km/s.

Using Eq. A3 to write $\hat{\mathcal{W}}$ in terms of the crystal frame coordinates, we can easily find $\hat{\mathbf{q}} \cdot \mathbf{V}_{\rm EarthRot}$ as

$$\hat{\mathbf{q}} \cdot \mathbf{V}_{\rm EarthRot} = -V_{\rm RotEq}\cos\lambda_{\rm lab}\left(\beta_X q_X + \beta_Y q_Y + \beta_Z q_Z\right). \tag{B12}$$

There is no time dependence in Eq. B12, because it is written in the crystal frame, and both the lab and the crystal are rotating with the Earth.

5. Total Velocity

Now we can insert Eqs. B4, B6, B9 and B12 into Eq. B1 to compute $\hat{\mathbf{q}} \cdot \mathbf{V}_{\rm lab}$. Inserting the values of $V_\oplus = 29.8$ km/s, $\epsilon = 23.439^\circ$ and $V_{\rm RotEq} = 0.465$ km/s, we have (in km/s):

$$\begin{aligned}\hat{\mathbf{q}} \cdot \mathbf{V}_{\rm lab} = &\left\{ \left[-\cos(t^\circ_{\rm lab})\ A(t) + \sin(t^\circ_{\rm lab})\ B(t) \right] \sin\lambda_{\rm lab} + C(t)\ \cos\lambda_{\rm lab} \right\} (\alpha_X q_X + \alpha_Y q_Y + \alpha_Z q_Z) \\ &+ \left\{ \sin(t^\circ_{\rm lab})\ A(t) + \cos(t^\circ_{\rm lab})\ B(t) - 0.465 \cos\lambda_{\rm lab} \right\} (\beta_X q_X + \beta_Y q_Y + \beta_Z q_Z) \\ &+ \left\{ \left[\cos(t^\circ_{\rm lab})\ A(t) - \sin(t^\circ_{\rm lab})\ B(t) \right] \cos\lambda_{\rm lab} + C(t)\ \sin\lambda_{\rm lab} \right\} (\gamma_X q_X + \gamma_Y q_Y + \gamma_Z q_Z)\,, \end{aligned} \tag{B13}$$

where

$$\begin{aligned} A(t) &= 0.4927\ V_{\rm GalRot} - 1.066\ {\rm km/s} + (V_\oplus(\lambda(t))\mathcal{A}(t), \\ B(t) &= 0.4503\ V_{\rm GalRot} + 16.56\ {\rm km/s} - (V_\oplus(\lambda(t))\mathcal{B}(t), \\ C(t) &= 0.7445\ V_{\rm GalRot} + 7.077\ {\rm km/s} + (V_\oplus(\lambda(t))\mathcal{C}(t). \end{aligned} \tag{B14}$$

---

[1] E. M. Drobyshevski, Mod. Phys. Lett. A **23** (2008) 3077 [arXiv:0706.3095 [physics.ins-det]].

[2] R. Bernabei *et al.*, Eur. Phys. J. C **53**, 205 (2008) [arXiv:0710.0288 [astro-ph]].

[3] F. T. Avignone, R. J. Creswick and S. Nussinov, arXiv:0807.3758 [hep-ph]; R. J. Creswick, S. Nussinov and F. T. Avignone, arXiv:1007.0214v2 [astro-ph.IM].

[4] J. Lindhard, Kongel. Dan. Vidensk. Selsk., Mat.-Fys. Medd. **34** No. 14 (1965).

[5] N. Bozorgnia, G. B. Gelmini and P. Gondolo, JCAP **11**, 019 (2010) [arXiv:1006.3110 [astro-ph.CO]];

[6] N. Bozorgnia, G. B. Gelmini and P. Gondolo, JCAP **11**, 028 (2010) [arXiv:1008.3676 [astro-ph.CO]]; N. Bozorgnia, G. B. Gelmini and P. Gondolo, JCAP **11**, 029 (2010) [arXiv:1009.3325 [astro-ph.CO]]; N. Bozorgnia, G. B. Gelmini and P. Gondolo, arXiv:1011.6006 [astro-ph.CO].

[7] K. M. Górski *et al.*, ApJ **622**, 759 (2005).

[8] P. Gondolo, Phys. Rev. D **66**, 103513 (2002).

[9] M.S. Alenazi and P. Gondolo, Phys. Rev. D **77**, 043532 (2008).

[10] R. Helm, Phys. Rev. **104** 1466 (1956).

[11] G. Duda, A. Kemper, and P. Gondolo, JCAP 0704 012, **12** (2007).

[12] A. M. Green, JCAP **10** 034 (2010) [arXiv:1009.0916v2 [astro-ph.CO]].

[13] M. Kuhlen *et al.*, JCAP **02** 030 (2010) [arXiv:0912.2358v1 [astro-ph.GA]].

[14] R. Bernabei *et al.*, Eur. Phys. J. C **56** (2008) 333 [arXiv:0804.2741v1 [astro-ph]].

[15] R. Bernabei *et al.* [DAMA Collaboration], Nucl. Instrum. Meth. A **592**, 297 (2008) [arXiv:0804.2738 [astro-ph]].

[16] D. Hooper, J.I. Collar, J. Hall, D. McKinsey and C.M. Kelso, Phys. Rev. D **82** 123509 (2010) [arXiv:1007.1005v3 [hep-ph]].

[17] C. Savage, G. Gelmini, P. Gondolo and K. Freese, Phys. Rev. D **83** 055002 (2011) [arXiv:1006.0972v2 [astro-ph.CO]].

[18] Z. Ahmed *et al.* [CDMS Collaboration], Phys. Rev. Lett **106** 131302 (2011) [arXiv:1011.2482 [astro-ph.CO]].

[19] E. Aprile *et al.* [XENON100 Collaboration], arXiv:1104.2549v2 [astro-ph.CO].

[20] S. T. Lin *et al.* [TEXONO Collaboration], Phys. Rev. D **79** 061101 (2009) [arXiv:0712.1645 [hep-ex]]; C. E. Aalseth *et al.* [CoGeNT Collaboration], Phys. Rev. Lett. **101**, 251301 (2008) [Erratum-ibid. **102**, 109903 (2009)] [arXiv:0807.0879 [astro-ph]].

[21] V. I. Tretyak, Astropart. Phys **33** 40 (2010) [arXiv:0911.3041v1 [nucl-ex]].

[22] D. Hooper, J. I. Collar, J. Hall, D. McKinsey and C. Kelso, Phys. Rev. D **82** 123509 (2010) [arXiv:1007.1005v3 [hep-ph]].

[23] M. A. Hapgood, Planet. Space Sci. 40, 711 (1992).

[24] U.S. Naval Observatory, *Almanac for Computers* 1990. Nautical Almanac Office, U.S. Naval Observatory, Washington, D.C.

[25] Peter Duffett-Smith, "Practical Astronomy with Your Calculator", 3rd ed. Cambridge, England: Cambridge University Press (1992).

[26] R. Schoenrich, J. Binney and W. Dehnen, Mon. Not. Roy. Astron. Soc. **403** 1829 (2010) [arXiv:0912.3693].

[27] K. R. Lang, Astrophysical Formulae, Springer-Verlag, New York (1999).

[28] A. M. Green, Phys. Rev D **68** 023004 (2003).